

CERN-EP-2024-204
22 July 2024

Measurement of *CP* violation observables in $D^+ \rightarrow K^- K^+ \pi^+$ decays

LHCb collaboration[†]

Abstract

A search for violation of the charge-parity (*CP*) symmetry in the $D^+ \rightarrow K^- K^+ \pi^+$ decay is presented, with proton-proton collision data corresponding to an integrated luminosity of 5.4 fb^{-1} , collected at a center-of-mass energy of 13 TeV with the LHCb detector. A novel model-independent technique is used to compare the D^+ and D^- phase-space distributions, with instrumental asymmetries subtracted using the $D_s^+ \rightarrow K^- K^+ \pi^+$ decay as a control channel. The *p*-value for the hypothesis of *CP* conservation is 8.1%. The *CP* asymmetry observables $A_{CP|S}^{\phi\pi^+} = (0.95 \pm 0.43_{\text{stat}} \pm 0.26_{\text{syst}}) \times 10^{-3}$ and $A_{CP|S}^{\bar{K}^{*0}K^+} = (-0.26 \pm 0.56_{\text{stat}} \pm 0.18_{\text{syst}}) \times 10^{-3}$ are also measured. These results show no evidence of *CP* violation and represent the most sensitive search performed through the phase space of a multibody decay.

Submitted to Phys. Rev. Lett.

© 2024 CERN for the benefit of the LHCb collaboration. [CC BY 4.0 licence](#).

[†]Authors are listed at the end of this Letter.

The breaking of the combined charge-parity (CP) symmetry in particle interactions is a critical element in explaining the imbalance between matter and antimatter in the Universe [1]. Existing observations of CP violation in K and B meson decays are consistent with predictions from the Standard Model (SM), where the violation arises from a single irreducible phase in the Cabibbo–Kobayashi–Maskawa (CKM) quark mixing matrix [2, 3]. However, the effect of this phase alone is insufficient to explain the observed matter–antimatter asymmetry [4–7], underscoring the necessity for new CP -violating dynamics beyond the SM.

In the charm-quark sector, CP violation has so far only been observed in the difference between the time-integrated CP asymmetries of $D^0 \rightarrow \pi^- \pi^+$ and $D^0 \rightarrow K^- K^+$ decays [8]. These are Cabibbo-suppressed decays, with transitions of the type $c \rightarrow uq\bar{q}$ ($q = d, s$) for which the SM predicts very small CP asymmetries, of the order of 10^{-3} or less. The recent measurement of the asymmetry in the $D^0 \rightarrow K^- K^+$ decay [9, 10] indicates that the observed signal is mostly due to CP violation in the $D^0 \rightarrow \pi^- \pi^+$ decay amplitude. The interpretation of these results is still being debated, with explanations falling within the SM [11–14] and some suggesting physics beyond it [15–18]. Measurements of CP asymmetries in a wide range of decays are fundamental to fully exploit the potential of charmed hadrons for revealing signs of physics beyond the SM.

Three-body decays have unique features for CP -asymmetry studies. Depending on the underlying mechanism of CP violation, localized asymmetries across the decay phase-space can be considerably larger than the integrated value, as observed already in B^+ decays [19, 20]. The $D^+ \rightarrow K^- K^+ \pi^+$ decay¹ is the three-body Cabibbo-suppressed D^+ decay with the largest branching fraction [21]. Studies of CP violation across its Dalitz plot, a two-dimensional diagram representing the phase space [22, 23], have previously been undertaken by the BaBar [24], CLEO [25] and LHCb [26] collaborations. Measurements of the CP asymmetry in the phase-space region dominated by $D^+ \rightarrow \phi \pi^+$, with $\phi \rightarrow K^- K^+$, have also been reported by LHCb [27, 28]. All results are consistent with CP symmetry.

In this Letter, a search for localized CP violation in the phase space of $D^+ \rightarrow K^- K^+ \pi^+$ decays is presented, using data collected by the LHCb experiment from 2016 to 2018, corresponding to an integrated luminosity of 5.4 fb^{-1} . Currently, this represents the largest sample available of c -hadron decays with potential for observation of CP violation. A model-independent technique is developed to address the challenge of isolating the CP asymmetry from instrumental effects, by exploiting the control channel $D_s^+ \rightarrow K^- K^+ \pi^+$, for which CP violation is not expected [15, 29].

The LHCb detector is a single-arm forward spectrometer covering the pseudorapidity range $2 < \eta < 5$, described in detail in Refs. [30, 31]. It is designed for the study of particles containing b or c quarks. The magnetic field polarity is reversed periodically during data taking to mitigate the differences of reconstruction efficiencies of particles with opposite charges. Data sets corresponding to about one half of the total integrated luminosity are recorded with each magnetic field configuration.

The online event selection is performed by a trigger consisting of a hardware stage followed by a two-level software stage. In between the two software stages, an alignment and calibration of the detector is performed in near real-time and their results are used in the trigger [32]. In the first software stage, events used in this analysis are selected if at least one track has large transverse momentum and is incompatible with originating from

¹The inclusion of charge-conjugate processes is implied throughout except in the discussion of asymmetries.

any primary vertex (PV), or if any two-track combination forming a vertex significantly displaced from the PV is found in the event by a multivariate algorithm [33, 34]. In the second stage, two oppositely charged particles identified as kaons are combined with a particle identified as a pion to form a good-quality decay vertex detached from any PV. The PV with the smallest value of χ_{IP}^2 is associated with the decay candidate, where χ_{IP}^2 is defined as the difference in the vertex-fit χ^2 of the PV reconstructed with and without the particle under consideration, in this case, the $D_{(s)}^+$ candidate. Further requirements are applied on the $D_{(s)}^+$ decay time, on the angle between the reconstructed $D_{(s)}^+$ momentum vector and the vector connecting the PV to the decay vertex, on the χ^2 of the $D_{(s)}^+$ decay-vertex fit, and on the momentum, the transverse momentum and the χ_{IP}^2 of the $D_{(s)}^+$ candidate and of its decay products. The invariant masses of the D^+ and D_s^+ candidates are required to be within the intervals [1805,1935] MeV and [1905,2035] MeV, which correspond to approximately ten times their mass resolution.²

The candidates selected from the second software-trigger stage are directly used for the offline analysis [34] and must satisfy additional selection criteria, applied uniformly for the D^+ and D_s^+ samples whenever possible, to minimize potential biases in the CP violation study. A stringent particle identification (PID) requirement is applied on both kaons, which reduces to a negligible level the contamination from $D^+ \rightarrow K^- \pi^+ \pi^+$ decays in the $D_s^+ \rightarrow K^- K^+ \pi^+$ sample, while significantly reducing background due to random combinations of tracks. Contamination from semileptonic decays where the muon is misidentified as a pion is suppressed by a muon PID veto to the pion candidate. Contamination from $\Lambda_c^+ \rightarrow K^- p \pi^+$ decays and random combinations of $D^0 \rightarrow K^- \pi^+$ decays with a pion are removed using invariant-mass vetoes. The requirement on the maximum χ_{IP}^2 of the $D_{(s)}^+$ meson is further tightened to reduce the contamination from secondary b -hadron decays. Fiducial requirements are applied to remove small regions of the kinematic space where large charge asymmetries are observed, typically caused by low-momentum tracks being swept out of the detector acceptance by the magnetic field. Finally, candidates are randomly rejected to equalize, in each data-taking year, the signal yields of the samples collected with each magnet polarity.

After applying all selection criteria, the yields for D^+ and D_s^+ decays are approximately 135 and 181 million, respectively, with a purity of 95% within an interval of ± 20 MeV around their nominal masses. The $K^- K^+ \pi^+$ invariant-mass distributions are shown in Fig. 3 of the Appendix.

The strategy to identify a signal of CP violation in the $D^+ \rightarrow K^- K^+ \pi^+$ decay is a model-independent search based upon a χ^2 -test for the hypothesis of the charge asymmetries over the D^+ Dalitz plot being compatible with those of the D_s^+ control mode. It assumes that the nuisance asymmetries (*i.e.*, differences in charged-particle detection, reconstruction or selection efficiencies, left-right detector or any other instrumental asymmetries) depend only on the kinematics of the final-state particles and that local effects arising from correlations between the $D_{(s)}^+$ kinematic-dependent production asymmetries and the Dalitz plot variables are negligible, making the difference between the production asymmetries a global effect that can be subtracted.

The Dalitz plots are divided into bins and the raw charge asymmetry for the decay X

²Natural units with $c = 1$ are used throughout.

in each bin i is defined as

$$A_{\text{raw}}^{i,X} = \frac{N_+^{i,X} - N_-^{i,X}}{N_+^{i,X} + N_-^{i,X}}, \quad (1)$$

where $X = S, C$ refers to the signal (S) or control (C) modes, $+$ and $-$ refer to the charge of the $D_{(s)}^\pm$ candidates, and $N_{+(-)}^{i,X}$ is the number of decays $X_{+(-)}$ in bin i , as determined from mass fits described later. The CP observable is defined as

$$\Delta A_{CP}^i = A_{\text{raw}}^{i,S} - A_{\text{raw}}^{i,C} - \Delta A_{\text{raw}}^{\text{global}}. \quad (2)$$

The term $\Delta A_{\text{raw}}^{\text{global}}$ is the global difference in asymmetries averaged over all bins in the Dalitz plot,

$$\Delta A_{\text{raw}}^{\text{global}} = \frac{\sum_i^{N_{\text{bins}}} \frac{A_{\text{raw}}^{i,S} - A_{\text{raw}}^{i,C}}{\sigma_{A_{\text{raw}}^{i,S}}^2 + \sigma_{A_{\text{raw}}^{i,C}}^2}}{\sum_i^{N_{\text{bins}}} \frac{1}{\sigma_{A_{\text{raw}}^{i,S}}^2 + \sigma_{A_{\text{raw}}^{i,C}}^2}}, \quad (3)$$

where $\sigma_{A_{\text{raw}}^{i,X}}$ are the $A_{\text{raw}}^{i,X}$ uncertainties. Any difference between the global asymmetries in the two decays is cancelled by this term which, in the absence of CP violation, corresponds to the difference between the D^+ and D_s^+ production asymmetries. The $A_{\text{raw}}^{i,C}$ term cancels out instrumental asymmetries from the raw signal asymmetry in bin i .

To build the χ^2 test-statistic, the significance of ΔA_{CP}^i ,

$$\mathcal{S}_{\Delta CP}^i = \frac{\Delta A_{CP}^i}{\sigma_{\Delta A_{CP}^i}}, \quad (4)$$

is used, where $\sigma_{\Delta A_{CP}^i}$ is the ΔA_{CP}^i statistical uncertainty and accounts for the correlations between the individual per-bin asymmetries and the global difference of asymmetries. The expressions for $\sigma_{\Delta A_{CP}^i}$ and $\sigma_{\Delta A_{\text{raw}}^{\text{global}}}$ are presented in Eq. 7 and Eq. 8 in the Appendix. Under the hypothesis of CP symmetry, $\mathcal{S}_{\Delta CP}^i$ follows a standard normal distribution, as validated using pseudoexperiments.

The test-statistic is then defined as

$$\chi^2(\mathcal{S}_{\Delta CP}) = \sum_i^{N_{\text{bins}}} (\mathcal{S}_{\Delta CP}^i)^2, \quad (5)$$

from which a p -value for the hypothesis of no localized CP violation can be extracted.

The Dalitz plots for the signal and control samples are depicted in Fig. 1, where the binning scheme is overlaid. In this plot, $s(K^-\pi^+)$ and $s(K^-K^+)$ represent the squared invariant masses of the $K^-\pi^+$ and K^-K^+ systems, respectively. For the purpose of this plot, background subtraction is performed using the *sPlot* technique [35], based on D^+ and D_s^+ invariant-mass fits.

The binning scheme is designed to exploit the resonant structures in the $D^+ \rightarrow K^-K^+\pi^+$ decay, which are similar to those in the $D_s^+ \rightarrow K^-K^+\pi^+$ decay. Key features in these decays are the $\bar{K}^*(892)^0$ and $\phi(1020)$ vector resonances, prominently visible around $s(K^-\pi^+) = m_{\bar{K}^*0}^2$ and $s(K^-K^+) = m_\phi^2$. Vector resonance distributions in the Dalitz plot present a node, shown more explicitly in the inset of Fig. 1 for the ϕ case. The rectangular areas around the two resonances are divided into four bins with

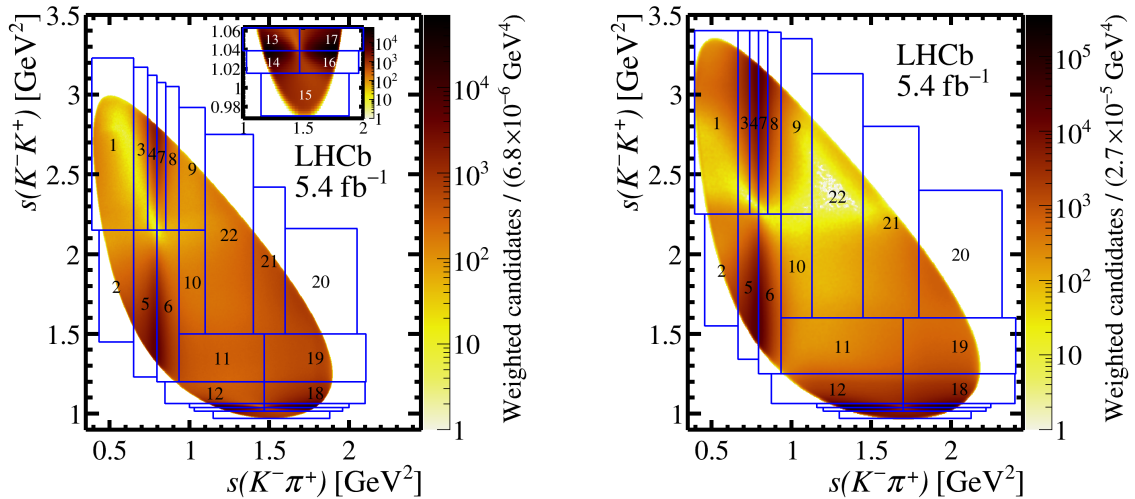


Figure 1: Dalitz plots for (left) $D^+ \rightarrow K^- K^+ \pi^+$ and (right) $D_s^+ \rightarrow K^- K^+ \pi^+$ decays in data with the binning scheme overlaid. The enlarged inset shows the bins around the $\phi\pi^+$ region, where the same numbering scheme is followed for both channels.

the internal boundaries defined by the distribution node in one direction and the known mass [21] in the other. For the K^{*0} resonance, the region above the node is further subdivided to account for instrumental asymmetry variations. Other Dalitz plot areas are segmented to approximately equalize the number of candidates in each bin, with the D_s^+ Dalitz plot following a similar segmentation with expanded outer limits. This design has a natural bin-to-bin correspondence between the Dalitz plots of D^+ and D_s^+ mesons with a good agreement between final-state kinematic quantities in each bin. A bin-by-bin weighting procedure is applied to the D_s^+ candidates to correct for residual differences.

Sensitivity studies, where $D^+ \rightarrow K^- K^+ \pi^+$ samples are generated according to the isobar model from Ref. [25], support this binning choice. In these studies, CP violation is introduced as small differences in the relative phase or magnitude of one or more resonances' amplitudes between the D^+ and D^- samples. The asymmetry caused by a phase difference changes sign when crossing vertically or horizontally between quadrants around the resonance of interest. This behavior motivates the measurement of the CP asymmetry observable $A_{CP|S}$ [27]:

$$A_{CP|S} = \frac{1}{2} [(\Delta A_{\text{raw}}^{\text{top-left}} + \Delta A_{\text{raw}}^{\text{bottom-right}}) - (\Delta A_{\text{raw}}^{\text{top-right}} + \Delta A_{\text{raw}}^{\text{bottom-left}})], \quad (6)$$

where $\Delta A_{\text{raw}} = A_{\text{raw}}^S - A_{\text{raw}}^C$ and the Dalitz plot bins top-left, top-right, bottom-left, and bottom-right are the ones numbered in Fig. 1 as bins 13, 17, 14 and 16 (3+4, 7+8, 5 and 6),³ respectively, for the $\phi\pi^+$ ($\bar{K}^{*0} K^+$) resonant amplitude. In this case, the global asymmetry components cancel out, making $A_{CP|S}$ an observable sensitive purely to CP violation in the decay. The local ΔA_{CP}^i are also provided as additional measurements, which can be interpreted as CP -violating observables in light of theoretical predictions, but only as relative quantities between bins. All the results from the present study are insensitive to CP violation manifested solely as a global asymmetry.

³The plus sign indicates that candidates from two bins are combined before computing $A_{CP|S}$.

To verify the method and mitigate experimenter’s bias, multiple tests were conducted before examining the $A_{\text{raw}}^{i,S}$ values. Both signal and control samples were segmented by $D_{(s)}^+$ momentum, pseudorapidity, and transverse momentum, confirming that ΔA_{CP}^i values were statistically compatible among these segments. Simulations [36] of the $D^+ \rightarrow K^- K^+ \pi^+$ and $D_s^+ \rightarrow K^- K^+ \pi^+$ decays, using a realistic resonant model with the same yields as in data, are used to study the impact of known effects, such as detection and tracking efficiency asymmetries [37] and PID efficiency asymmetries extracted from calibration samples [38], obtained as a function of the kaon and pion kinematics. The patterns of asymmetries in simulated signal and control samples match those observed in the control data. Additionally, various production-asymmetry models are tested, based on the results obtained with data taken in 2011 and 2012 [39–41]. None of the models significantly affects the local raw asymmetry patterns across the Dalitz plot. The method’s validity is further confirmed through 10,000 pseudoexperiments designed to simulate instrumental asymmetries, with the resulting $\sum_i^{N_{\text{bins}}} (\mathcal{S}_{\Delta CP}^i)^2$ values fitting a χ^2 distribution with N_{bins} degrees of freedom.

The signal and background raw charge asymmetries and yields are directly determined for each Dalitz plot bin from simultaneous χ^2 fits to the binned $K^\mp K^\pm \pi^\pm$ invariant-mass distributions of $D_{(s)}^+$ and $D_{(s)}^-$ candidates, independently for each data taking year and magnet polarity. The raw asymmetries are then combined for the final results. The signal and background shapes, as well as the procedure used to verify that the extracted asymmetries are unbiased, are described in the Appendix.

The results for ΔA_{CP}^i are shown in detail in Table 1. Systematic uncertainties arise from various sources and are evaluated by comparing results obtained with alternative procedures to the nominal ones. The impact of remaining kinematic mismatches between the control and signal samples is assessed by obtaining the D_s^+ asymmetries without equalization weights. Different fit models for the signal and background mass shapes are tested. Biases due to differences in the instrumental asymmetries related to the different D^+ and D_s^+ lifetimes, flight distance distributions and contamination from b -hadron decays, which cannot be disentangled, are determined by splitting the samples into two ranges of D -meson flight distance significance and χ_{IP}^2 and combining the resulting ΔA_{CP}^i values. For most bins, this is the dominant systematic uncertainty (labelled as “sec.dec.” in Table 1). The influence of different requirements in the trigger for the signal and control channels is investigated by aligning the selection criteria. The precision in each bin is limited by the statistical uncertainty. A graphical representation of the results is shown in Fig. 4 of the Appendix.

The CP observables $A_{CP|S}$ for the $\phi\pi^+$ and $\bar{K}^{*0}K^+$ systems are given by

$$\begin{aligned} A_{CP|S}^{\phi\pi^+} &= (0.95 \pm 0.43 \pm 0.26) \times 10^{-3}, \\ A_{CP|S}^{\bar{K}^{*0}K^+} &= (-0.26 \pm 0.56 \pm 0.18) \times 10^{-3}, \end{aligned}$$

where the first uncertainty is statistical and the second is systematic, evaluated using the same procedure described for the ΔA_{CP}^i results. The uncertainties are also shown in detail in Table 1.

Finally, the statistical significances $\mathcal{S}_{\Delta CP}^i$ are shown across the Dalitz plot in Fig. 2. The χ^2 of the search test is 31.8 for 22 degrees of freedom, resulting in a p -value of 8.1%, consistent with the hypothesis of no localized CP violation in the phase space of the $D^+ \rightarrow K^- K^+ \pi^+$ decay. Potential systematic biases in the search test results are

Table 1: Experimental results for $\Delta A_{CP}^i = \Delta A_{\text{raw}}^i - \Delta A_{\text{raw}}^{\text{global}}$ and $A_{CP|S}$, with systematic and statistical uncertainties shown in the last two columns. The individual contributions to the systematic uncertainties are also shown. All values are expressed in 10^{-3} units.

Bin	ΔA_{CP}	$\sigma_{\text{syst}}^{\text{weighting}}$	$\sigma_{\text{syst}}^{\text{sec.dec.}}$	$\sigma_{\text{syst}}^{\text{fit}}$	$\sigma_{\text{syst}}^{\text{trigger}}$	$\sigma_{\text{syst}}^{\text{tot}}$	σ_{stat}
1	1.97	0.67	1.35	0.88	0.10	1.75	1.39
2	0.78	0.32	0.19	0.50	0.26	0.68	1.33
3	-0.01	0.01	0.49	0.15	0.67	0.85	1.43
4	0.06	0.20	0.11	0.24	0.21	0.39	0.75
5	0.24	0.06	0.07	0.04	0.05	0.11	0.36
6	0.71	0.05	0.21	0.08	0.17	0.29	0.38
7	0.99	0.06	0.36	0.19	0.04	0.41	0.73
8	0.69	0.16	0.57	0.13	0.13	0.63	1.28
9	-3.14	0.99	0.60	1.59	0.01	1.97	2.49
10	0.83	1.28	1.97	2.63	0.87	3.63	1.97
11	-0.02	0.20	0.39	0.10	0.24	0.51	0.78
12	1.08	0.11	0.22	0.11	0.03	0.27	0.63
13	0.25	0.04	0.13	0.06	0.06	0.17	0.42
14	-0.99	0.08	0.05	0.07	0.08	0.14	0.42
15	-1.99	0.01	0.56	0.08	0.18	0.60	0.90
16	0.12	0.05	0.26	0.07	0.15	0.31	0.43
17	-0.55	0.08	0.08	0.10	0.03	0.15	0.35
18	-0.24	0.19	0.39	0.03	0.14	0.46	0.47
19	-0.53	0.07	0.50	0.20	0.34	0.64	0.75
20	-2.14	0.46	0.29	0.29	0.20	0.65	1.14
21	0.45	0.48	0.53	0.23	0.42	0.86	1.07
22	2.14	1.28	1.09	0.81	0.85	2.05	2.23
Resonant mode	$A_{CP S}$	$\sigma_{\text{syst}}^{\text{weighting}}$	$\sigma_{\text{syst}}^{\text{sec.dec.}}$	$\sigma_{\text{syst}}^{\text{fit}}$	$\sigma_{\text{syst}}^{\text{trigger}}$	$\sigma_{\text{syst}}^{\text{tot}}$	σ_{stat}
$\phi\pi^+$	0.95	0.12	0.21	0.07	0.07	0.26	0.43
$\bar{K}^{*0}K^+$	-0.26	0.01	0.16	0.06	0.06	0.18	0.56

examined by evaluating ΔA_{CP}^i in the same alternative scenarios used to evaluate systematic uncertainties for ΔA_{CP}^i . The resulting p -values range from 2.3% to 14.1%, confirming absence of localized CP violation over the Dalitz plot within the current statistical reach.

In summary, this Letter reports a search for CP violation across the phase space of $D^+ \rightarrow K^- K^+ \pi^+$ decays utilizing a novel binned, model-independent method that neutralizes instrumental effects via a control channel with an identical final state. The p -values, obtained from all considered scenarios, are consistent with CP symmetry. The observables ΔA_{CP}^i are measured with 10^{-3} precision within the bins of the Dalitz plot. This constitutes the most precise search for localized CP violation ever performed. Furthermore, this study presents the most precise measurement of $A_{CP|S}^{\phi\pi^+}$ and the first experimental result for $A_{CP|S}^{\bar{K}^{*0}K^+}$, both compatible with zero with a precision smaller than 10^{-3} .

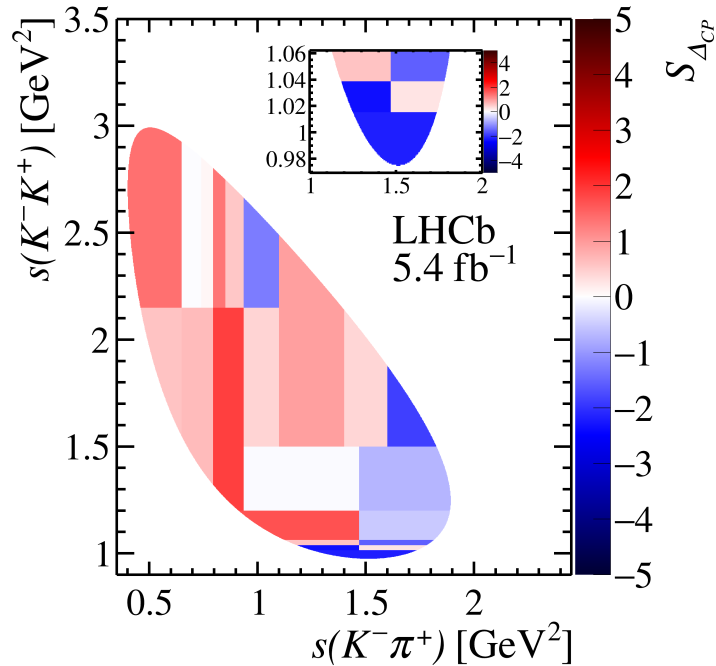


Figure 2: The significance $\mathcal{S}_{\Delta_{CP}}$ across the Dalitz plot, which accounts only for the statistical uncertainty. The inset shows a zoom of the Dalitz plot around the $\phi\pi^+$ region.

Acknowledgements

We express our gratitude to our colleagues in the CERN accelerator departments for the excellent performance of the LHC. We thank the technical and administrative staff at the LHCb institutes. We acknowledge support from CERN and from the national agencies: CAPES, CNPq, FAPERJ and FINEP (Brazil); MOST and NSFC (China); CNRS/IN2P3 (France); BMBF, DFG and MPG (Germany); INFN (Italy); NWO (Netherlands); MNiSW and NCN (Poland); MCID/IFA (Romania); MICIU and AEI (Spain); SNSF and SER (Switzerland); NASU (Ukraine); STFC (United Kingdom); DOE NP and NSF (USA). We acknowledge the computing resources that are provided by CERN, IN2P3 (France), KIT and DESY (Germany), INFN (Italy), SURF (Netherlands), PIC (Spain), GridPP (United Kingdom), CSCS (Switzerland), IFIN-HH (Romania), CBPF (Brazil), and Polish WLCG (Poland). We are indebted to the communities behind the multiple open-source software packages on which we depend. Individual groups or members have received support from ARC and ARDC (Australia); Key Research Program of Frontier Sciences of CAS, CAS PIFI, CAS CCEPP, Fundamental Research Funds for the Central Universities, and Sci. & Tech. Program of Guangzhou (China); Minciencias (Colombia); EPLANET, Marie Skłodowska-Curie Actions, ERC and NextGenerationEU (European Union); A*MIDEX, ANR, IPhU and Labex P2IO, and Région Auvergne-Rhône-Alpes (France); AvH Foundation (Germany); ICSC (Italy); Severo Ochoa and María de Maeztu Units of Excellence, GVA, XuntaGal, GENCAT, InTalent-Inditex and Prog. Atracción Talento CM (Spain); SRC (Sweden); the Leverhulme Trust, the Royal Society and UKRI (United Kingdom).

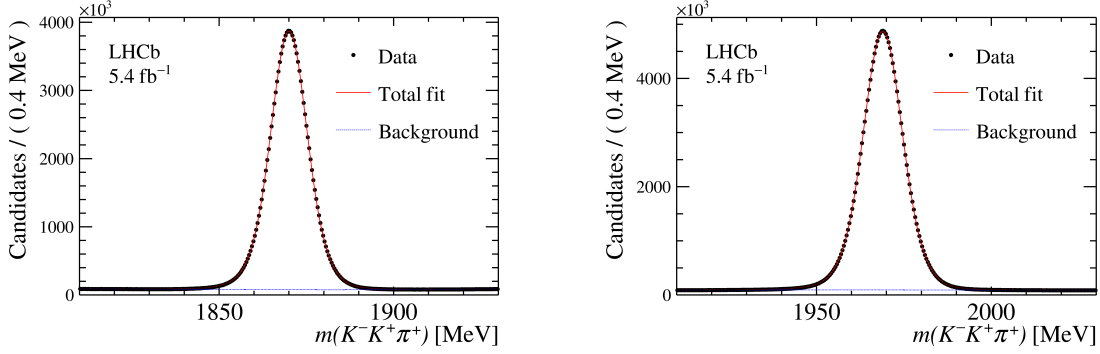


Figure 3: Invariant-mass distribution of the final samples of (left) $D^+ \rightarrow K^- K^+ \pi^+$ and (right) $D_s^+ \rightarrow K^- K^+ \pi^+$ candidates.

A Appendix

A.1 Invariant-mass distributions and fits

The probability density function (PDF) used to describe the $K^\mp K^\pm \pi^\pm$ invariant-mass distribution of signal candidates in each bin of the Dalitz plot is given by a sum of a Gaussian function and a double-sided Crystal Ball (DSCB) function [42], with widths and tails that can differ between the left and right sides of the PDF around the most probable value. All the parameters describing the signal shape, apart from the Gaussian width and mean, are fixed to the values obtained from simulation, weighted by PID efficiencies obtained from calibration samples [38]. The fixed parameters are the offset and relative fraction between the DSCB and the Gaussian functions, and the tail parameters of the DSCB. The background is parameterized by a third-order Bernstein polynomial for $D^+ \rightarrow K^- K^+ \pi^+$ and as a second-order for polynomial for $D_s^+ \rightarrow K^- K^+ \pi^+$ decays. The Gaussian width and the background parameters are shared between the $D_{(s)}^+$ and $D_{(s)}^-$ subsamples that are fitted simultaneously.

The fits are validated using pseudoexperiments, where $K^\mp K^\pm \pi^\pm$ invariant-mass distributions are generated according to the baseline fit results and then fitted with the same prescription. The pulls for the fitted parameters follow standard normal distributions across all Dalitz plot bins for both decay modes. This analysis confirms that the signal and background asymmetries are unbiased.

For illustration, the mass distributions of the $D^+ \rightarrow K^- K^+ \pi^+$ and $D_s^+ \rightarrow K^- K^+ \pi^+$ candidates, summed over all Dalitz plots bins, are given in Fig. 3.

A.2 Uncertainties of the observables

The statistical uncertainties of the asymmetries defined in the Letter are shown below for completeness.

$$\sigma_{\Delta A_{CP}^i} = \sqrt{\left(1 - \frac{\sigma_{\Delta A_{\text{raw}}^{\text{global}}}^2}{\sigma_{A_{\text{raw}}^i, S}^2 + \sigma_{A_{\text{raw}}^i, C}^2}\right)^2 (\sigma_{A_{\text{raw}}^i, S}^2 + \sigma_{A_{\text{raw}}^i, C}^2) + \sigma_{\Delta A_{\text{raw}}^{\text{global}}}^4 \sum_{j \neq i}^{N_{\text{bins}}} \frac{1}{\sigma_{A_{\text{raw}}^j, S}^2 + \sigma_{A_{\text{raw}}^j, C}^2}} \quad (7)$$

$$\sigma_{\Delta A_{\text{raw}}^{global}} = \left[\sum_i^{N_{bins}} \frac{1}{\sigma_{A_{\text{raw}}^{i,S}}^2 + \sigma_{A_{\text{raw}}^{i,C}}^2} \right]^{-\frac{1}{2}} \quad (8)$$

A.3 Graphical representation of the CP asymmetries

A graphical representation of the ΔA_{CP}^i results is shown in Fig. 4. The horizontal axis is given by the bin index, according to the scheme depicted in Fig. 1.

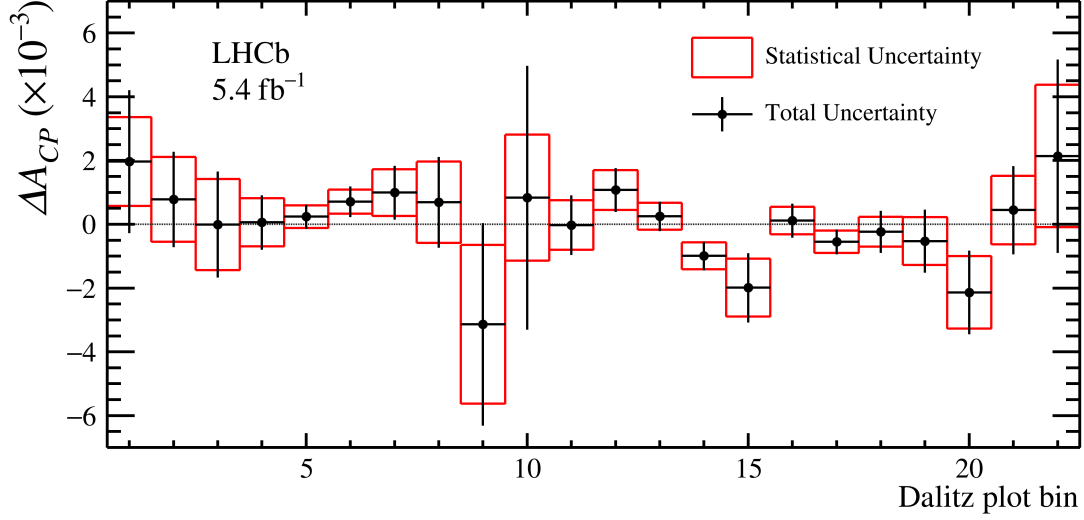







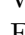
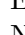
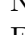
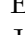

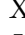






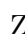
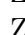
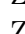
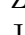
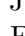
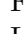
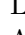
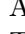
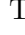
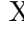
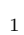
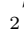
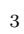

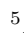
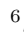


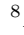
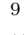
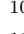
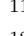
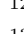
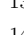

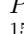
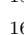
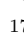
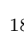
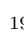
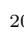
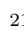
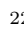
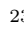
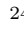
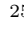
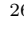







Figure 4: Difference of charge asymmetries ΔA_{CP}^i for each bin of the Dalitz plot.

References

- [1] A. D. Sakharov, *Violation of CP invariance, C asymmetry, and baryon asymmetry of the universe*, *Pisma Zh. Eksp. Teor. Fiz.* **5** (1967) 32.
- [2] N. Cabibbo, *Unitary symmetry and leptonic decays*, *Phys. Rev. Lett.* **10** (1963) 531.
- [3] M. Kobayashi and T. Maskawa, *CP-violation in the renormalizable theory of weak interaction*, *Prog. Theor. Phys.* **49** (1973) 652.
- [4] M. B. Gavela *et al.*, *Standard model CP violation and baryon asymmetry. Part 2: Finite temperature*, *Nucl. Phys.* **B430** (1994) 382, [arXiv:hep-ph/9406289](#).
- [5] M. B. Gavela, P. Hernandez, J. Orloff, and O. Pène, *Standard model CP violation and baryon asymmetry*, *Mod. Phys. Lett.* **A9** (1994) 795, [arXiv:hep-ph/9312215](#).
- [6] A. G. Cohen, D. B. Kaplan, and A. E. Nelson, *Progress in electroweak baryogenesis*, *Annual Review of Nuclear and Particle Science* **43** (1993) 27.
- [7] A. Riotto and M. Trodden, *Recent progress in baryogenesis*, *Annual Review of Nuclear and Particle Science* **49** (1999) 35.
- [8] LHCb collaboration, R. Aaij *et al.*, *Observation of CP violation in charm decays*, *Phys. Rev. Lett.* **122** (2019) 211803, [arXiv:1903.08726](#).
- [9] LHCb collaboration, R. Aaij *et al.*, *Measurement of the time-integrated CP asymmetry in $D^0 \rightarrow K^- K^+$ decays*, *Phys. Rev. Lett.* **131** (2023) 091802, [arXiv:2209.03179](#).
- [10] LHCb collaboration, *Simultaneous determination of the CKM angle γ and parameters related to mixing and CP violation in the charm sector*, [LHCb-CONF-2024-004](#), 2024; LHCb collaboration, R. Aaij *et al.*, *Simultaneous determination of CKM angle γ and charm mixing parameters*, *JHEP* **12** (2021) 141, [arXiv:2110.02350](#).
- [11] Y. Grossman and S. Schacht, *The emergence of the $\Delta U = 0$ rule in charm physics*, *JHEP* **07** (2019) 020, [arXiv:1903.10952](#).
- [12] H.-Y. Cheng and C.-W. Chiang, *Revisiting CP violation in $D \rightarrow PP$ and VP decays*, *Phys. Rev.* **D100** (2019) 093002, [arXiv:1909.03063](#).
- [13] S. Schacht and A. Soni, *Enhancement of charm CP violation due to nearby resonances*, *Phys. Lett.* **B825** (2022) 136855, [arXiv:2110.07619](#).
- [14] I. Bediaga, T. Frederico, and P. C. Magalhães, *Enhanced charm CP asymmetries from final state interactions*, *Phys. Rev. Lett.* **131** (2023) 051802, [arXiv:2203.04056](#).
- [15] Y. Grossman, A. L. Kagan, and Y. Nir, *New physics and CP violation in singly Cabibbo suppressed D decays*, *Phys. Rev.* **D75** (2007) 036008, [arXiv:hep-ph/0609178](#).
- [16] A. Khodjamirian and A. A. Petrov, *Direct CP asymmetry in $D \rightarrow \pi^- \pi^+$ and $D \rightarrow K^- K^+$ in QCD-based approach*, *Phys. Lett.* **B774** (2017) 235, [arXiv:1706.07780](#).

- [17] A. Pich, E. Solomonidi, and L. Vale Silva, *Final-state interactions in the CP asymmetries of charm-meson two-body decays*, *Phys. Rev.* **D108** (2023) 036026, [arXiv:2305.11951](#).
- [18] A. Lenz, M. L. Piscopo, and A. V. Rusov, *Two body non-leptonic D^0 decays from LCSR and implications for Δa_{CP}^{dir}* , *JHEP* **03** (2024) 151, [arXiv:2312.13245](#).
- [19] LHCb collaboration, R. Aaij *et al.*, *Observation of several sources of CP violation in $B^+ \rightarrow \pi^+\pi^+\pi^-$ decays*, *Phys. Rev. Lett.* **124** (2020) 031801, [arXiv:1909.05211](#).
- [20] LHCb collaboration, R. Aaij *et al.*, *Direct CP violation in charmless three-body decays of B^\pm mesons*, *Phys. Rev.* **D108** (2023) 012008, [arXiv:2206.07622](#).
- [21] Particle Data Group, R. L. Workman *et al.*, *Review of particle physics*, *Prog. Theor. Exp. Phys.* **2022** (2022) 083C01.
- [22] R. H. Dalitz, *On the analysis of τ -meson data and the nature of the τ -meson*, *Phil. Mag. Ser. 7* **44** (1953) 1068.
- [23] E. Fabri, *A study of τ -meson decay*, *Nuovo Cim.* **11** (1954) 479.
- [24] BaBar collaboration, B. Aubert *et al.*, *A search for CP violation and a measurement of the relative branching fraction in $D^+ \rightarrow K^-K^+\pi^+$ decays*, *Phys. Rev.* **D71** (2005) 091101, [arXiv:hep-ex/0501075](#).
- [25] CLEO Collaboration, P. Rubin *et al.*, *Search for CP violation in the Dalitz-plot analysis of $D^\pm \rightarrow K^+K^-\pi^\pm$* , *Phys. Rev.* **D78** (2008) 072003, [arXiv:0807.4545](#).
- [26] LHCb collaboration, R. Aaij *et al.*, *Search for CP violation in $D^+ \rightarrow K^-K^+\pi^+$ decays*, *Phys. Rev.* **D84** (2011) 112008, [arXiv:1110.3970](#).
- [27] LHCb collaboration, R. Aaij *et al.*, *Search for CP violation in $D^+ \rightarrow \phi\pi^+$ and $D_s^+ \rightarrow K_S^0\pi^+$ decays*, *JHEP* **06** (2013) 112, [arXiv:1303.4906](#).
- [28] LHCb collaboration, R. Aaij *et al.*, *Search for CP violation in $D_s^+ \rightarrow K_S^0\pi^+$, $D^+ \rightarrow K_S^0K^+$ and $D^+ \rightarrow \phi\pi^+$ decays*, *Phys. Rev. Lett.* **122** (2019) 191803, [arXiv:1903.01150](#).
- [29] I. Bediaga and C. Göbel, *Direct CP violation in beauty and charm hadron decays*, *Progress in Particle and Nuclear Physics* **114** (2020) 103808, [arXiv:2009.07037](#).
- [30] LHCb collaboration, A. A. Alves Jr. *et al.*, *The LHCb detector at the LHC*, *JINST* **3** (2008) S08005.
- [31] LHCb collaboration, R. Aaij *et al.*, *LHCb detector performance*, *Int. J. Mod. Phys.* **A30** (2015) 1530022, [arXiv:1412.6352](#).
- [32] G. Dujany and B. Storaci, *Real-time alignment and calibration of the LHCb Detector in Run II*, *J. Phys. Conf. Ser.* **664** (2015) 082010.
- [33] R. Aaij *et al.*, *The LHCb trigger and its performance in 2011*, *JINST* **8** (2013) P04022, [arXiv:1211.3055](#).

- [34] R. Aaij *et al.*, *Tesla: an application for real-time data analysis in high energy physics*, *Comput. Phys. Commun.* **208** (2016) 35, [arXiv:1604.05596](#).
- [35] M. Pivk and F. R. Le Diberder, *sPlot: A statistical tool to unfold data distributions*, *Nucl. Instrum. Meth.* **A555** (2005) 356, [arXiv:physics/0402083](#).
- [36] G. A. Cowan, D. C. Craik, and M. D. Needham, *RapidSim: an application for the fast simulation of heavy-quark hadron decays*, *Comput. Phys. Commun.* **214** (2017) 239, [arXiv:1612.07489](#).
- [37] A. Davis *et al.*, *Measurement of the instrumental asymmetry for $K^- \pi^+$ -pairs at LHCb in Run 2*, [LHCb-PUB-2018-004](#), [CERN-LHCb-PUB-2018-004](#), 2018.
- [38] R. Aaij *et al.*, *Selection and processing of calibration samples to measure the particle identification performance of the LHCb experiment in Run 2*, *Eur. Phys. J. Tech. Instr.* **6** (2019) 1, [arXiv:1803.00824](#).
- [39] LHCb collaboration, R. Aaij *et al.*, *Measurement of the D^\pm production asymmetry in 7 TeV pp collisions*, *Phys. Lett.* **B718** (2013) 902, [arXiv:1210.4112](#).
- [40] LHCb collaboration, R. Aaij *et al.*, *Measurement of the $D_s^+ - D_s^-$ production asymmetry in 7 TeVpp collisions*, *Phys. Lett.* **B713** (2012) 186, [arXiv:1205.0897](#).
- [41] LHCb collaboration, R. Aaij *et al.*, *Measurement of D_s^\pm production asymmetry in pp collisions at $\sqrt{s} = 7$ and 8 TeV*, *JHEP* **08** (2018) 008, [arXiv:1805.09869](#).
- [42] T. Skwarnicki, *A study of the radiative cascade transitions between the Upsilon-prime and Upsilon resonances*, PhD thesis, Institute of Nuclear Physics, Krakow, 1986, [DESY-F31-86-02](#).

G. Valenti²³ , N. Valls Canudas⁴⁷ , H. Van Hecke⁶⁶ , E. van Herwijnen⁶⁰ ,
C.B. Van Hulse^{45,w} , R. Van Laak⁴⁸ , M. van Veghel³⁶ , G. Vasquez⁴⁹ ,
R. Vazquez Gomez⁴⁴ , P. Vazquez Regueiro⁴⁵ , C. Vázquez Sierra⁴⁵ , S. Vecchi²⁴ ,
J.J. Velthuis⁵³ , M. Veltri^{25,v} , A. Venkateswaran⁴⁸ , M. Vesterinen⁵⁵ , D.
Vico Benet⁶² , P. V. Vidrier Villalba⁴⁴ , M. Vieites Diaz⁴⁷ , X. Vilasis-Cardona⁴³ ,
E. Vilella Figueras⁵⁹ , A. Villa²³ , P. Vincent¹⁵ , F.C. Volle⁵² , D. vom Bruch¹² ,
N. Voropaev⁴² , K. Vos⁷⁷ , G. Vouters^{10,47} , C. Vrahas⁵⁷ , J. Wagner¹⁸ , J. Walsh³³ ,
E.J. Walton^{1,55} , G. Wan⁶ , C. Wang²⁰ , G. Wang⁸ , J. Wang⁶ , J. Wang⁵ ,
J. Wang⁴ , J. Wang⁷² , M. Wang²⁸ , N. W. Wang⁷ , R. Wang⁵³ , X. Wang⁸,
X. Wang⁷⁰ , X. W. Wang⁶⁰ , Y. Wang⁶ , Z. Wang¹³ , Z. Wang⁴ , Z. Wang²⁸ ,
J.A. Ward^{55,1} , M. Waterlaet⁴⁷ , N.K. Watson⁵² , D. Websdale⁶⁰ , Y. Wei⁶ ,
J. Wendel⁷⁹ , B.D.C. Westhenry⁵³ , C. White⁵⁴ , M. Whitehead⁵⁸ , E. Whiter⁵² ,
A.R. Wiederhold⁵⁵ , D. Wiedner¹⁸ , G. Wilkinson⁶² , M.K. Wilkinson⁶⁴ ,
M. Williams⁶³ , M.R.J. Williams⁵⁷ , R. Williams⁵⁴ , Z. Williams⁵³ , F.F. Wilson⁵⁶ ,
W. Wislicki⁴⁰ , M. Witek³⁹ , L. Witola²⁰ , C.P. Wong⁶⁶ , G. Wormser¹³ ,
S.A. Wotton⁵⁴ , H. Wu⁶⁷ , J. Wu⁸ , Y. Wu⁶ , Z. Wu⁷ , K. Wyllie⁴⁷ , S. Xian⁷⁰,
Z. Xiang⁵ , Y. Xie⁸ , A. Xu³³ , J. Xu⁷ , L. Xu⁴ , L. Xu⁴ , M. Xu⁵⁵ , Z. Xu⁴⁷ ,
Z. Xu⁷ , Z. Xu⁵ , D. Yang , K. Yang⁶⁰ , S. Yang⁷ , X. Yang⁶ , Y. Yang^{27,l} ,
Z. Yang⁶ , Z. Yang⁶⁵ , V. Yeroshenko¹³ , H. Yeung⁶¹ , H. Yin⁸ , C. Y. Yu⁶ ,
J. Yu⁶⁹ , X. Yuan⁵ , Y. Yuan^{5,7} , E. Zaffaroni⁴⁸ , M. Zavertyaev¹⁹ , M. Zdybal³⁹ ,
F. Zenesini^{23,i} , C. Zeng^{5,7} , M. Zeng⁴ , C. Zhang⁶ , D. Zhang⁸ , J. Zhang⁷ ,
L. Zhang⁴ , S. Zhang⁶⁹ , S. Zhang⁶² , Y. Zhang⁶ , Y. Z. Zhang⁴ , Y. Zhao²⁰ ,
A. Zharkova⁴² , A. Zhelezov²⁰ , S. Z. Zheng⁶ , X. Z. Zheng⁴ , Y. Zheng⁷ ,
T. Zhou⁶ , X. Zhou⁸ , Y. Zhou⁷ , V. Zhovkovska⁵⁵ , L. Z. Zhu⁷ , X. Zhu⁴ ,
X. Zhu⁸ , V. Zhukov¹⁶ , J. Zhuo⁴⁶ , Q. Zou^{5,7} , D. Zuliani^{31,o} , G. Zunica⁴⁸ .

¹*School of Physics and Astronomy, Monash University, Melbourne, Australia*

²*Centro Brasileiro de Pesquisas Físicas (CBPF), Rio de Janeiro, Brazil*

³*Universidade Federal do Rio de Janeiro (UFRJ), Rio de Janeiro, Brazil*

⁴*Center for High Energy Physics, Tsinghua University, Beijing, China*

⁵*Institute Of High Energy Physics (IHEP), Beijing, China*

⁶*School of Physics State Key Laboratory of Nuclear Physics and Technology, Peking University, Beijing, China*

⁷*University of Chinese Academy of Sciences, Beijing, China*

⁸*Institute of Particle Physics, Central China Normal University, Wuhan, Hubei, China*

⁹*Consejo Nacional de Rectores (CONARE), San Jose, Costa Rica*

¹⁰*Université Savoie Mont Blanc, CNRS, IN2P3-LAPP, Annecy, France*

¹¹*Université Clermont Auvergne, CNRS/IN2P3, LPC, Clermont-Ferrand, France*

¹²*Aix Marseille Univ, CNRS/IN2P3, CPPM, Marseille, France*

¹³*Université Paris-Saclay, CNRS/IN2P3, IJCLab, Orsay, France*

¹⁴*Laboratoire Leprince-Ringuet, CNRS/IN2P3, Ecole Polytechnique, Institut Polytechnique de Paris, Palaiseau, France*

¹⁵*LPNHE, Sorbonne Université, Paris Diderot Sorbonne Paris Cité, CNRS/IN2P3, Paris, France*

¹⁶*I. Physikalisches Institut, RWTH Aachen University, Aachen, Germany*

¹⁷*Universität Bonn - Helmholtz-Institut für Strahlen und Kernphysik, Bonn, Germany*

¹⁸*Fakultät Physik, Technische Universität Dortmund, Dortmund, Germany*

¹⁹*Max-Planck-Institut für Kernphysik (MPIK), Heidelberg, Germany*

²⁰*Physikalisches Institut, Ruprecht-Karls-Universität Heidelberg, Heidelberg, Germany*

²¹*School of Physics, University College Dublin, Dublin, Ireland*

²²*INFN Sezione di Bari, Bari, Italy*

²³*INFN Sezione di Bologna, Bologna, Italy*

²⁴*INFN Sezione di Ferrara, Ferrara, Italy*

²⁵*INFN Sezione di Firenze, Firenze, Italy*

²⁶*INFN Laboratori Nazionali di Frascati, Frascati, Italy*

- ²⁷ INFN Sezione di Genova, Genova, Italy
- ²⁸ INFN Sezione di Milano, Milano, Italy
- ²⁹ INFN Sezione di Milano-Bicocca, Milano, Italy
- ³⁰ INFN Sezione di Cagliari, Monserrato, Italy
- ³¹ INFN Sezione di Padova, Padova, Italy
- ³² INFN Sezione di Perugia, Perugia, Italy
- ³³ INFN Sezione di Pisa, Pisa, Italy
- ³⁴ INFN Sezione di Roma La Sapienza, Roma, Italy
- ³⁵ INFN Sezione di Roma Tor Vergata, Roma, Italy
- ³⁶ Nikhef National Institute for Subatomic Physics, Amsterdam, Netherlands
- ³⁷ Nikhef National Institute for Subatomic Physics and VU University Amsterdam, Amsterdam, Netherlands
- ³⁸ AGH - University of Krakow, Faculty of Physics and Applied Computer Science, Kraków, Poland
- ³⁹ Henryk Niewodniczanski Institute of Nuclear Physics Polish Academy of Sciences, Kraków, Poland
- ⁴⁰ National Center for Nuclear Research (NCBJ), Warsaw, Poland
- ⁴¹ Horia Hulubei National Institute of Physics and Nuclear Engineering, Bucharest-Magurele, Romania
- ⁴² Affiliated with an institute covered by a cooperation agreement with CERN
- ⁴³ DS4DS, La Salle, Universitat Ramon Llull, Barcelona, Spain
- ⁴⁴ ICCUB, Universitat de Barcelona, Barcelona, Spain
- ⁴⁵ Instituto Galego de Física de Altas Enerxías (IGFAE), Universidade de Santiago de Compostela, Santiago de Compostela, Spain
- ⁴⁶ Instituto de Física Corpuscular, Centro Mixto Universidad de Valencia - CSIC, Valencia, Spain
- ⁴⁷ European Organization for Nuclear Research (CERN), Geneva, Switzerland
- ⁴⁸ Institute of Physics, Ecole Polytechnique Fédérale de Lausanne (EPFL), Lausanne, Switzerland
- ⁴⁹ Physik-Institut, Universität Zürich, Zürich, Switzerland
- ⁵⁰ NSC Kharkiv Institute of Physics and Technology (NSC KIPT), Kharkiv, Ukraine
- ⁵¹ Institute for Nuclear Research of the National Academy of Sciences (KINR), Kyiv, Ukraine
- ⁵² School of Physics and Astronomy, University of Birmingham, Birmingham, United Kingdom
- ⁵³ H.H. Wills Physics Laboratory, University of Bristol, Bristol, United Kingdom
- ⁵⁴ Cavendish Laboratory, University of Cambridge, Cambridge, United Kingdom
- ⁵⁵ Department of Physics, University of Warwick, Coventry, United Kingdom
- ⁵⁶ STFC Rutherford Appleton Laboratory, Didcot, United Kingdom
- ⁵⁷ School of Physics and Astronomy, University of Edinburgh, Edinburgh, United Kingdom
- ⁵⁸ School of Physics and Astronomy, University of Glasgow, Glasgow, United Kingdom
- ⁵⁹ Oliver Lodge Laboratory, University of Liverpool, Liverpool, United Kingdom
- ⁶⁰ Imperial College London, London, United Kingdom
- ⁶¹ Department of Physics and Astronomy, University of Manchester, Manchester, United Kingdom
- ⁶² Department of Physics, University of Oxford, Oxford, United Kingdom
- ⁶³ Massachusetts Institute of Technology, Cambridge, MA, United States
- ⁶⁴ University of Cincinnati, Cincinnati, OH, United States
- ⁶⁵ University of Maryland, College Park, MD, United States
- ⁶⁶ Los Alamos National Laboratory (LANL), Los Alamos, NM, United States
- ⁶⁷ Syracuse University, Syracuse, NY, United States
- ⁶⁸ Pontifícia Universidade Católica do Rio de Janeiro (PUC-Rio), Rio de Janeiro, Brazil, associated to ³
- ⁶⁹ School of Physics and Electronics, Hunan University, Changsha City, China, associated to ⁸
- ⁷⁰ Guangdong Provincial Key Laboratory of Nuclear Science, Guangdong-Hong Kong Joint Laboratory of Quantum Matter, Institute of Quantum Matter, South China Normal University, Guangzhou, China, associated to ⁴
- ⁷¹ Lanzhou University, Lanzhou, China, associated to ⁵
- ⁷² School of Physics and Technology, Wuhan University, Wuhan, China, associated to ⁴
- ⁷³ Departamento de Física, Universidad Nacional de Colombia, Bogota, Colombia, associated to ¹⁵
- ⁷⁴ Ruhr Universitaet Bochum, Fakultae f. Physik und Astronomie, Bochum, Germany, associated to ¹⁸
- ⁷⁵ Eotvos Lorand University, Budapest, Hungary, associated to ⁴⁷
- ⁷⁶ Van Swinderen Institute, University of Groningen, Groningen, Netherlands, associated to ³⁶
- ⁷⁷ Universiteit Maastricht, Maastricht, Netherlands, associated to ³⁶
- ⁷⁸ Tadeusz Kosciuszko Cracow University of Technology, Cracow, Poland, associated to ³⁹

- ⁷⁹ *Universidade da Coruña, A Coruna, Spain, associated to* ⁴³
- ⁸⁰ *Department of Physics and Astronomy, Uppsala University, Uppsala, Sweden, associated to* ⁵⁸
- ⁸¹ *University of Michigan, Ann Arbor, MI, United States, associated to* ⁶⁷
- ⁸² *Departement de Physique Nucleaire (SPhN), Gif-Sur-Yvette, France*
- ^a *Universidade de Brasília, Brasília, Brazil*
- ^b *Centro Federal de Educação Tecnológica Celso Suckow da Fonseca, Rio De Janeiro, Brazil*
- ^c *Hangzhou Institute for Advanced Study, UCAS, Hangzhou, China*
- ^d *School of Physics and Electronics, Henan University, Kaifeng, China*
- ^e *LIP6, Sorbonne Université, Paris, France*
- ^f *Universidad Nacional Autónoma de Honduras, Tegucigalpa, Honduras*
- ^g *Università di Bari, Bari, Italy*
- ^h *Università di Bergamo, Bergamo, Italy*
- ⁱ *Università di Bologna, Bologna, Italy*
- ^j *Università di Cagliari, Cagliari, Italy*
- ^k *Università di Ferrara, Ferrara, Italy*
- ^l *Università di Genova, Genova, Italy*
- ^m *Università degli Studi di Milano, Milano, Italy*
- ⁿ *Università degli Studi di Milano-Bicocca, Milano, Italy*
- ^o *Università di Padova, Padova, Italy*
- ^p *Università di Perugia, Perugia, Italy*
- ^q *Scuola Normale Superiore, Pisa, Italy*
- ^r *Università di Pisa, Pisa, Italy*
- ^s *Università della Basilicata, Potenza, Italy*
- ^t *Università di Roma Tor Vergata, Roma, Italy*
- ^u *Università di Siena, Siena, Italy*
- ^v *Università di Urbino, Urbino, Italy*
- ^w *Universidad de Alcalá, Alcalá de Henares, Spain*
- ^x *Facultad de Ciencias Físicas, Madrid, Spain*
- ^y *Department of Physics/Division of Particle Physics, Lund, Sweden*
- [†] *Deceased*